Full Paper

Propellants, Explosives, Pyrotechnics

DOI: 10.1002/prep.201900032

Validation of a Multi-Dimensional Model for Unsteady Combustion of AP/HTPB Propellants

Carmen López-Munoz,*[a] Francisco-Javier Sánchez Velasco,[a] José-Ramón García-Cascales,[a] Ramón Mur,[b] and Ramón-Antonio Otón-Martínez[c]

Abstract: In this work, a model for the characterization of unsteady combustion of AP/HTPB composite propellants is benchmarked against experimental data. The model describes a change of phase of the propellant from condensed to gas phase and afterwards its combustion by a simplified chemistry scheme. A Finite Volume approximation is used to solve the system of equations. Firstly, the conservation equations including all source terms but combustion source terms are solved, in this case the numerical fluxes are computed by using Rusanov numerical scheme. Diffusive source terms are solved explicitly. After this, a first order Euler scheme is used to solve the system of ordinary differential equations resulting after considering the combustion source terms. The code is validated with two tests: the burning of a strand composed by AP and HTPB in sandwich configuration and the burning of a strand composed by AP particles uniformly distributed within HTPB. In both cases, simulation results are compared with experimental data. Influence of the pressure in burning rate, AP mass fraction, temperature and gas velocity are examined for sandwich test. For the strand, the effect of the pressure and initial temperature is also analyzed. Results show a good agreement between experimental and numerical data.

Keywords: Combustion · Composite propellants · Multi-dimensional modelling · AP/HTPB · Experimental validation

1 Introduction

Composite solid propellants are heterogeneous mixtures of crystalline oxidizer and polymer fuel binder with some other additives. Modelling the combustion of composite propellants is a key problem that has focused the interest of several researches in many industrial fields such as chemical engineering, aerospace engineering or safety in industrial processes. Kuo and Summerfield [1] made a review of some classical models used to characterize the combustion of this type of materials. Among those models, BDP model [2] was developed to describe the combustion of ammonium perchlorate (AP)-based composite propellants. It defines three separate flame zones: i) a primary flame consisting in the reactions of binder and oxidizer decomposition products, ii) a premixed oxidizer flame and iii) a final diffusion flame involving the products of the other two flames. This one-dimensional (1D) model considers simple global chemical kinetics for the reactions of the gas phase whereas the surface decomposition of the propellant ingredients is described by simple Arrhenius expressions. In general terms, the calculated burning rate, surface temperature and temperature sensitivity obtained with this model got a fair agreement with experimental data.

The PEM (petite ensemble model), similar to BDP, is another example of classical combustion model for composite propellants which considers the existence of different small flames associated with the distribution of particles sizes of AP [1]. In contrast to these classical models, there are currently available other complex models based on detailed chemical kinetics for the combustion of AP-based propellants. For example, in the case of AP composite propellants mixed with hydroxyl-terminated polybutadiene (HTPB) as inert binder, it is noteworthy the detailed combustion mechanism proposed by Jeppson and Beckstead [3]. In that work, the authors presented a full kinetic mechanism based on 72 reactions and 44 species for the gas phase and a semi-global mechanism consisting of 8 steps for condensed phase decomposition. The model accurately describes burn rate versus pressure data for low to moderate pressure ranges. In addition to the classic and the complex combustion models, there are several alternatives in the literature based on simplified combustion mechanisms with reduced chemistry kinetics. Among them, the works of Guirao and Williams [4], Knott and Brewster [5], Cao et al. [6], Cai and

[a] C. López-Munoz, F.-J. Sánchez Velasco, J.-R. García-Cascales
Department of Fluid Mechanics and Thermal Engineering
Universidad Politécnica de Cartagena
Dr.Fleming, s/n. 30202, Cartagena, Murcia, Spain
*e-mail: carmen.lopez@upct.es
[b] R. Mur
EXPAL Systems S.A. (MAXAM Defence)
Avda. del Partenón, 16, 28042 Madrid, Spain
[c] R.-A. Otón-Martínez
University Centre of Defence at the Spanish Air Force Academy (MDE-UPCT)
Academia General del Aire, Calle Coronel López Peña, s/n. 30720, Santiago de la Ribera, Murcia, Spain

Yang [7] and Cai et al. [8] stand out. The model of Guirao and Williams [4] assumes a one-step, second-order gas-phase reaction deduced from a 14-step gas-phase mechanism. A Lewis number of unity is considered in the gas phase. Their calculations suggest that 70% of AP is decomposed at the surface by condensed-phase reactions and the remaining 30% vaporizes into ammonia (NH_3) and perchloric acid $(HClO_4)$. Knott and Brewster [5] developed a two-dimensional model, able to capture the flame structure proposed by BDP and limited to steady state conditions, to describe the combustion of an AP (NH_4ClO_4) sandwich with two layers HTPB (HC) binder assuming a two-step global reaction. The model considers energy and species balance as governing equations for both gas and condensed phase. Energy and species conservation and temperature continuity are considered at the inter-phase surface to couple both phases. Cai et al. [7,8] developed a 2D model for the combustion of AP/HTPB in sandwich configuration for rocket-motor environments. The model uses a two-step global chemical reaction mechanism similar to the one adopted by Knott and Brewster [5] taking into account the governing equations for both gas and condensed phases. The model was used to examine erosive burning under cross-flow laminar conditions and to analyze the flame regime in terms of the Damköhler number (Da) in a rocket-motor chamber. Finally, the model proposed by Cao et al. [6], considers energy conservation equation for condensed phase and mass, momentum, energy and species governing equations for gas phase which is treated as ideal gas being viscous terms included in momentum conservation equation. The reaction mechanism is similar to Knott and Brewster [5].

Regarding experimental insights into the combustion dynamics of AP propellants, attention may be drawn to the work of Moriñigo et al. [9] in which the combustion dynamics of HTPB with oxygen in a wind tunnel is studied by comparing qualitatively the experimental data obtained with numerical simulations performed with LES. In that work, they propose a reduced chemical model with 2 steps and another model with 6 steps. Yu et al. [10] also show results of depressurization tests representing pressure evolution with time and burned mass. In addition, Kohga [11] provides experimental results of burning AP/HTPB composite propellant with and without the use of additives for low and high pressures and AP content from 20% to 80%. Moreover, Kohga [11] considers the influence of AP size in the burning rate by comparing the results obtained when using particles diameters of 4 μm and 110 μm. Not only Kohga [11], but also Jeppson and Beckstead [3], studied this effect by choosing AP grains with diameters from 20 μm to 200 μm and plotting the burning rate results for each one of them. Kubota [12] also mentioned the influence that the AP particle size has on the burning rate. The three authors remarked that, considering the same propellant composition, the smaller the particle size, the higher burning rate.

Finally, it is worth remarking that, in case of AP/HTPB propellants, several authors, such as Miccio [13] and Favale and Miccio [14], have pointed out that it is mandatory to consider the two-dimensional (2D) and/or the three-dimensional (3D) aspects of the problem due the involvement of diffusion flames. Therefore, it seems of major importance to develop multidimensional models to study the burning of this type of propellants, especially in the case of transient combustion. In this work, a transient multidimensional numerical model to describe the combustion of AP/HTPB propellant is presented in order to characterize temperature and species concentration. In addition, the study of the burning rate sensitivity to pressure and initial temperature variations is also one of the main objectives of the present work. The study is structured as follows, in section 2 the model and numerical method are described. Afterwards, results are presented in section 3. Finally, in section 4, conclusions are discussed and future work lines are outlined.

2 Experimental Section

2.1 Physical Model

The combustion of AP/HTPB propellant was modelled by considering a solid phase zone (hereafter cited as condensed phase) and a gas phase zone, which includes air, AP and HTPB in their gaseous forms and the combustion products. Both zones were assumed to be insulated excepting the surface in contact with the gas phase which is called burning surface.

The combustion mechanism was divided in two physicochemical processes, as described by Knott and Brewster [5] and Cai et al. [8]. Firstly, the change of phase of AP/HTPB propellant from condensed to gas form at the burning surface and secondly, the combustion of the propellant in gas phase. According to Cai et al. [8], the change of phase of the solid propellant takes place when the temperature of the condensed phase at the burning surface is higher than the melting temperature (T_{melt}), which for AP is defined around 830 K. Knott and Brewster [5] chemical kinetic scheme was employed to model the combustion of AP and HTPB in their gaseous form. The scheme is described by a two-step reaction mechanism as,

$$NH_4ClO_4 \rightarrow 1.25O_2 + \underbrace{1.5H_2O + HCl + 0.5N_2}_{P_1} \ (R1) \tag{1}$$

$$HC + 1.25O_2 + P_1 \rightarrow CO_2 + 0.5H_2O + P_1 \ (R2) \tag{2}$$

2.1.1 Governing Equations

The mathematical model applied to describe the combustion problem considers mass, momentum, energy and species mass fraction governing equations for the gas phase and energy equation for the solid phase:

$$\frac{\partial \rho_g}{\partial t} + \vec{\nabla}(\rho_g \vec{u}_g) = 0 \tag{3}$$

$$\frac{\partial (\rho_g \vec{u}_g)}{\partial t} + \vec{\nabla}\left(\rho_g \vec{u}_g \otimes \vec{u}_g + p\vec{I}\right) = 0 \tag{4}$$

$$\frac{\partial (\rho_g E_g)}{\partial t} + \vec{\nabla}\left(\rho_g \vec{u}_g \left(E_g + \frac{p}{\rho_g}\right)\right) = k_g \nabla^2 T_g + \sum_{N}^{j=1} Q_{g,j} R_j \tag{5}$$

$$\frac{\partial (\rho_g Y_i)}{\partial t} + \vec{\nabla}(\rho_g \vec{u}_g Y_i) = \frac{k_g}{\gamma_g c_{vg}} \nabla^2 Y_i + \phi_i \tag{6}$$

$$\frac{\partial (\rho_c E_c)}{\partial t} = k_c \nabla^2 T_c \tag{7}$$

where the subscript -i stands for the i-specie from 1 to n-1 and j stands for reaction number from 1 to N.

2.1.2 Burning Surface Coupling

In order to couple both phases together, the following boundary conditions are established:

1. Gas and solid temperature must be the same and equal to the surface temperature (T_s),

$$T_g = T_c = T_s \tag{8}$$

2. The heat that the gas transfers to the burning surface is invested firstly, in raising the surface temperature to produce the phase change and secondly, in warming the condensed phase by conduction. Therefore, the required energy balance at the burning surface is defined as,

$$k_g \nabla T_g\big|_s = k_c \nabla T_c\big|_s + \rho_c \dot{r}(Q_c - c_c(T_s - T_0)) \tag{9}$$

3. The continuity of mass must be ensured. Therefore, the following relationship is set,

$$u_{g,s} = \begin{cases} \frac{\rho_c \dot{r}}{\rho_g}, & T_s > T_{melt} \\ 0, & T_s < T_{melt} \end{cases} \tag{10}$$

4. Finally, species conservation must be ensured too

$$\rho_c \dot{r} Y_{s,i} = \rho_c \dot{r} Y_{c,i}\big|_{0^-} + \frac{k_g}{\gamma_g c_{vg}} \nabla Y_i\big|_{0^+} \tag{11}$$

Equations (9) to (11) show how the temperature, gas velocity and species mass fractions at the burning surface depend on the burning rate. As it can be seen in the following section, the burning rate of both AP and HTPB are function of the pressure and temperature of condensed and gas phases and therefore, dependent of the experimental conditions.

2.1.3 Source Terms

The closure laws to solve the equation system (3)–(7) are the state equation of gases, the burning rates of AP and HTPB and the reaction rates.

The gases were assumed ideal in this model and therefore, the equation of state is,

$$p = \rho_g R_g T_g \tag{12}$$

Specific constant of gases for a mixture of gases was calculated as follows,

$$R_g = R_u \sum_{n}^{i=0} Y_i / M_{g,i} \tag{13}$$

Similar formula was applied to calculate specific heat at constant volume,

$$c_{vg} = \sum_{n}^{i=0} Y_i c_{vg,i} \tag{14}$$

AP and HTPB combustion reactions (1) and (2) are described by its own reaction rate as,

$$R_1 = D_1 p^{n_1} Y_{AP} e^{\left(-\frac{E_1}{R_u T_g}\right)} \tag{15}$$

$$R_2 = D_2 p^{n_2} Y_{HTPB} Y_{O_2} e^{\left(-\frac{E_2}{R_u T_g}\right)} \tag{16}$$

According to Cai et al. [8] the burning rate is function of the pressure. Therefore, the burning rate calculation results,

$$\frac{Q_{g,1}}{2c_{AP}T_s}\dot{r}_{AP}^2 + \frac{k_g(T_g - T_s)}{d\rho_{AP}c_{AP}T_s}\dot{r}_{AP} = \frac{\alpha_{AP}}{\rho_{AP}}\left(\frac{D_1 p^{n_1} e^{\left(-\frac{E_1}{R_u T_g}\right)}}{\frac{E_1}{R_u T_g}}\right)\frac{Q_{g,1}}{Q_{c,AP}} \tag{17}$$

$$\frac{Q_{g,2}}{2c_{HTPB}T_s}\dot{r}_{HTPB}^2 + \frac{k_g(T_g - T_s)}{d\rho_{HTPB}c_{HTPB}T_s}\dot{r}_{HTPB} = \frac{\alpha_{HTPB}}{\rho_{HTPB}}\left(\frac{D_2 p^{n_2} e^{\left(-\frac{E_2}{R_u T_g}\right)}}{\frac{E_2}{R_u T_g}}\right)\frac{Q_{g,2}}{Q_{c,HTPB}} \tag{18}$$

2.2 Numerical Method

2.2.1 Numerical Method Proposed to Solve Gas Phase Equation System

The system of equations for gas phase can be written in vector form as:

$$\frac{\partial \boldsymbol{U}}{\partial t} + \nabla \cdot \mathcal{H} = \boldsymbol{S}_1(\boldsymbol{U}) + \boldsymbol{S}_2(\boldsymbol{U}) \tag{19}$$

where $(\boldsymbol{U})$ is the conserved variables vector, $(\mathcal{H})$ is the flux tensor and $(\boldsymbol{S})$ the source terms are split into two parts, $\boldsymbol{S}_1(\boldsymbol{U})$ with the diffusive terms and $\boldsymbol{S}_2(\boldsymbol{U})$ with the combustion terms, which are written below,

$$\boldsymbol{U} = \begin{pmatrix} \rho_g \\ \rho_g \vec{u}_g \\ \rho_g E_g \\ \rho_g Y_i \end{pmatrix}, \tag{20}$$

$$\mathcal{H} = \begin{pmatrix} \rho_g \vec{u}_g \\ \rho_g \vec{u}_g \otimes \vec{u}_g + p\vec{I} \\ \rho_g \vec{u}_g \left(E_g + \frac{p}{\rho_g} \right) \\ \rho_g \vec{u}_g Y_i \end{pmatrix}, \tag{21}$$

$$\mathbf{S}_1(\mathbf{U}) = \begin{pmatrix} 0 \\ 0 \\ k_g \nabla^2 T_g \\ \frac{k_g}{\gamma_g c_{vg}} \nabla^2 Y_i \end{pmatrix}, \tag{22}$$

$$\mathbf{S}_2(\mathbf{U}) = \begin{pmatrix} 0 \\ 0 \\ \sum_{j=1}^{N} Q_{gj} R_j \\ \phi_i \end{pmatrix} \tag{23}$$

To solve the equation system (19) a Finite Volume approach was used. The integration of the homogeneous part of this system in a control volume Ω yields,

$$\frac{\partial}{\partial t} \iiint_{\Omega} \boldsymbol{U} d\Omega + \iint_{A} \mathcal{H} \hat{n} dA = 0 \tag{24}$$

where A is the boundary of Ω and $\hat{n}$ is the normal vector to surface A. Considering the first integral as a time-rate of change of the averaging of the conserved variables $\boldsymbol{U}$ and the boundary A formed by N surfaces so that $A = \sum_{s=1}^{N} A_s$, equation (24) can be written as,

$$\frac{\partial \boldsymbol{U}}{\partial t} + \frac{1}{|\Omega|} \sum_{s=1}^{N} \iint_{A_s} \mathcal{H} \hat{n} dA = 0 \tag{25}$$

If the time derivative of the conserved variables is discretized as $\frac{\mathbf{U}_j^{n+1} - \mathbf{U}_j^n}{\Delta t}$, making use of the Rotational property $\mathcal{H}\hat{n} = \overline{T}_s^{-1} \boldsymbol{F}\left(\overline{T}_s \mathbf{U}\right)$ and the surface integral of the flux is approached by $\iint_A \mathcal{H} \hat{n} dA \approx \overline{T}_S^{-1} \boldsymbol{F}(\overline{T}_S \mathbf{U}) A_S$ a finite volume scheme for multiple dimensions in unstructured grids is obtained,

$$\boldsymbol{U}_j^{n+1} = \boldsymbol{U}_j^n - \frac{\Delta t}{|\Omega|} \sum_{s=1}^{N} \overline{T}_s^{-1} \boldsymbol{F}(\overline{T}_s \mathbf{U}) A_s \tag{26}$$

where $\overline{T}_s$ is the rotation matrix, $\overline{T}_s^{-1}$ its inverse and A_s is the area of the s^{th} surface bounding volume Ω.

The system of equations (26) was solved in two steps [15] as explained below,

1. Firstly, the complete equation system without the combustion source terms is solved,

$$\frac{\partial \boldsymbol{U}}{\partial t} + \nabla \cdot \mathcal{H} = \boldsymbol{S}_1(\boldsymbol{U}) \tag{27}$$

The Finite Volume approach adopted is

$$\overline{\boldsymbol{U}}_j^{n+1} = \boldsymbol{U}_j^n - \frac{\Delta t}{|\Omega|} \sum_{s=1}^{N} \overline{T}_s^{-1} \boldsymbol{F}(\overline{T}_s \mathbf{U}) A_s + \Delta t \boldsymbol{S}_1 \left(\boldsymbol{U}_j^n \right) \tag{28}$$

where the numerical flux has been computed by solving approximately the Riemann problem at each interface and the source term has been evaluated at (t_n) leaving the scheme explicit.

2. Next, the ODE

$$\frac{\partial \boldsymbol{U}}{\partial t} = \boldsymbol{S}_2(\boldsymbol{U}) \tag{29}$$

which considers, as mentioned, the source terms associated to the combustion process it is solved by using a first-order Euler method,

$$\boldsymbol{U}_j^{n+1} = \overline{\boldsymbol{U}}_j^{n+1} + \Delta t_{\text{chem}} \, \overline{\boldsymbol{S}}_{2,j}^{n+1} \tag{30}$$

The numerical flux of system (28) is evaluated by Rusanov scheme [16] as,

$$\boldsymbol{F}_{j+1/2}^n = \frac{1}{2} (\boldsymbol{F}_L + \boldsymbol{F}_R - S^+ (\boldsymbol{U}_R - \boldsymbol{U}_L)) \tag{31}$$

being S^+,

$$S^{+} = max\{|u_L - c_L|, |u_R - c_R|, |u_L + c_L|, |u_R + c_R|\} \quad (32)$$

where R and L stand for right and left respectively.

2.2.2 Time Integration

The time step considered to solve equation (28) was calculated as,

$$\Delta t = CFL \cdot min\left[min\left(\frac{\Delta x_j}{|\vec{u}_g| + c_g}\right)\right] \quad (33)$$

where the speed of sound c_g is calculated as,

$$c_g = \sqrt{\gamma_g R_g T_g} \quad (34)$$

On the other hand, to solve equation (30), the time step was obtained using the procedure detailed in García-Cascales et al. [17]. The calculation consists in defining small steps associated to chemical reaction until those small time steps equal the flux time step calculated in equation (33) as explained below,

1. A value of Δt very small and smaller than flux time is imposed.

2. Reaction rates R_1 and R_2, for AP and HTPB respectively, are calculated with the primitive values obtained from equation system (28).

3. With these reaction rates, a value of time step associated to the i-species consumed in j-reaction is calculated as follows,

$$\Delta t_{chem,i,j} = \frac{\rho_g Y_i}{\left|R_j coef_{i,j} \frac{M_{g,i}}{M_{g,j}}\right|} \quad (35)$$

where i stands for the i-species and j for reaction and $coef_{i,j}$ was defined as,

$$coef_{i,j} = coef_{i-p,j} - coef_{i-r,j} \quad (36)$$

being $coef_{i-p,j}$ the stechiometric coefficient of the i-specie in j-reaction as product, and $coef_{i-r,j}$ the stechiometric coefficient of the i-specie in j-reaction as reactive. There will be as many $\Delta t_{chem,i,j}$ as consumed species in j-reactions. From all those the smallest one is chosen (Δt_{chem}).

4. The chemical time (Δt_{chem}) is compared with that imposed initially. In case it is smaller, it is used to solve equation (30), if not, the initial time step will be used to solve the equation.

5. Equation (30) is solved and primitive variables are updated.

6. Remaining time is calculated in first iteration as the difference between total flux time step and the calculated chemical time step,

$$\Delta t_{remaining} = \Delta t - \Delta t_{chem} \quad (37)$$

in following iterations, the remaining time will be calculated as,

$$\Delta t_{remaining} = \Delta t_{remaining} - \Delta t_{chem} \quad (38)$$

7. The primitive variables calculated in after solving equation (30) are used to estimate again the reaction rates and with them the chemical time step of each species using equation (35). If the smallest chemical time step (Δt_{chem}) is smaller than the remaining flux time step $(\Delta t_{remaining})$, Δt_{chem} is used to solve equation (30) again. This process is repeated until the calculated chemical time step is higher than the remaining flux time step.

8. When this happens, the remaining flux time step is the one used to solve equation (30) and the calculation goes to the next convective Δt according to equation (33).

2.2.3 Numerical Method to Solve Condensed Phase Governing Equation

To obtain approximate solution to equation (7) Finite Volume method was used. Equation (7) can be written in vector form as,

$$\frac{\partial U}{\partial t} = S(U) \quad (39)$$

Where

$$U = \rho_c E_c \quad (40)$$

and

$$S(U) = k_c \nabla^2 T_c \quad (41)$$

In order to solve equation (39) first-order Euler method was used,

$$\overline{\boldsymbol{U}}_j^{n+1} = \boldsymbol{U}_j^n + \Delta t \boldsymbol{S}_j^n \quad (42)$$

2.3 Experimental Set-Up

In order to validate the model previously described, the code was programmed in C++ using OpenFoam and run for two different tests in two dimensions. The first one is the burning of a strand composed by AP and HTPB in sandwich configuration. This test is proposed by Cao et al. [6] who use the results provided by Kohga [11] to validate their code. Kohga [11] provides experimental results for the burning of strands of AP/HTPB propellant with AP particle diameter of 110 μm and several AP contents in a pressure range of 0.5–7 MPa. The second one is the burning of an AP/HTPB homogeneous strand. In this case the results are compared with data from experiments run in the facilities of National Spanish Institute of Aerospace Technology (INTA) [18] which test consists in the burning of an AP/HTPB strand from EXPAL Systems (R&D Department) of 4 mm in diameter and 155 mm in length in a Crawford Bomb Strand Burner for several room temperatures and in a pressure range from 4 to 19 MPa.

Thermophysical and chemical kinetic properties of composite AP/HTPB propellant were considered as input variables (see Table 1). These values are taken from Zhou et al. [19] and Ye et al. [20].

Table 1. Chemical kinetics and thermophysical properties of AP/HTPB composite propellant.

Parameter	Unit	AP	HTPB
n		1.744	1.750
D	$kg \cdot m^{-3} \cdot s^{-1} \cdot Pa^{-n}$	$2.261 \cdot 10^{-2}$	$2.294 \cdot 10^{-2}$
Q_g	$J \cdot kg^{-1}$	$1.799 \cdot 10^{6}$	$9.606 \cdot 10^{6}$
$E_{1,2}/R_u$	K^{-1}	8000	11000
ρ	$kg \cdot m^{-3}$	1950	920
k	$W \cdot m^{-1} \cdot K^{-1}$	0.405	0.276
Q_c	$J \cdot kg^{-1}$	$4.186 \cdot 10^{5}$	$1.967 \cdot 10^{5}$
M_g	$kg \cdot mol^{-1}$	0.1174	0.0130
c	$J \cdot kg^{-1} \cdot K^{-1}$	1255.2	1255.2

2.3.1 Sandwich configuration

In order to validate the model, an AP/HTPB propellant with 80% of AP content and particle average size of 110 μm was used for calculation, as described in Cao et al. [6].

The geometry used (Figure 1) is the one described by Ye et al. [20] which consist in a tube in which half of its volume is air and the other half is AP/HTPB composite propellant in sandwich configuration as in Cao et al. [6]. According to them, the width of the domain can be obtained using the following equation,

$$L = d_{AP} + d_{HTPB} \tag{43}$$

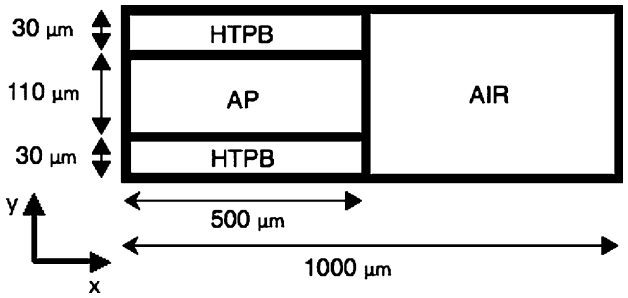

Figure 1. Geometry of AP/HTPB sandwich configuration.

where d_{AP} is the particle diameter of AP and d_{AP} is the width of HTPB which can be obtained from,

$$\frac{\rho_{AP} \cdot d_{AP}}{\rho_{HTPB} \cdot d_{HTPB}} = \frac{\alpha}{1-\alpha} \tag{44}$$

In this case the width of HTPB obtained was 60 mm therefore, the width of the domain was 170 μm. Both condensed and gas phase were considered 500 μm height.

Initial conditions of temperature are described by considering that the left side of the tube is set at 300 K (T_1) and the right side at 1315 K (T_2) increasing the temperature linearly. Initial temperature (T_0) and melting temperature (T_{melt}) are taken as 300 K and 800 K respectively.

2.3.2 Test tube in Crawford Bomb Strand Burner

The second test run to validate the code is the burning of an AP/HTPB strand for several room temperatures at 4 MPa and 7 MPa. The results are compared with those obtained in INTA facilities in which a strand of AP/HTPB of 4 mm in diameter and 155 mm in length.

The geometry simulated in this test (see Figure 2) was a tube of 156 mm in length and 4 mm in width in which 155 mm were considered homogeneous propellant with 74.41% of AP and 25.59% of HTPB and the rest was considered air.

The test was run for 4 MPa and 7 MPa and initial temperatures of −53 °C, 21 °C and 74 °C.

3 Results and Discussion

3.1 Sandwich Configuration

The code was run in 2D configuration for a pressure range from 0.5 MPa to 7 MPa. Distributions of temperature in condensed and in gas phases, AP mass fraction, velocity and pressure as well as burning rates for the already mentioned pressure range were obtained.

To validate the code, the comparison between the burning rate obtained using the model and the experimental re-

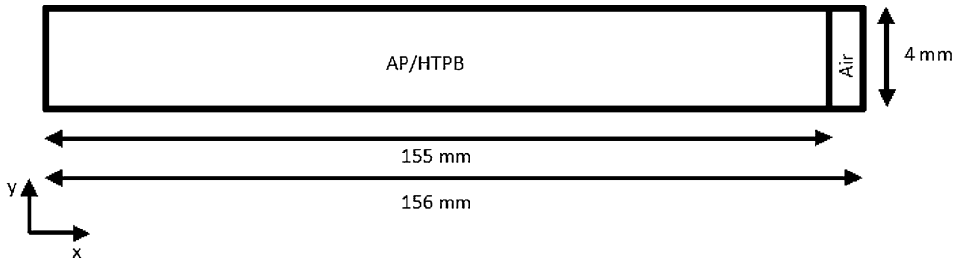

Figure 2. Geometry of AP/HTPB strand configuration.

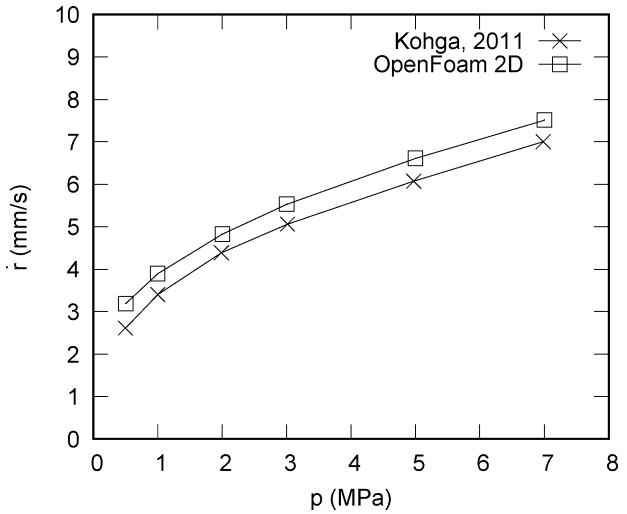

Figure 3. Comparison of calculated and experimental burning rate.

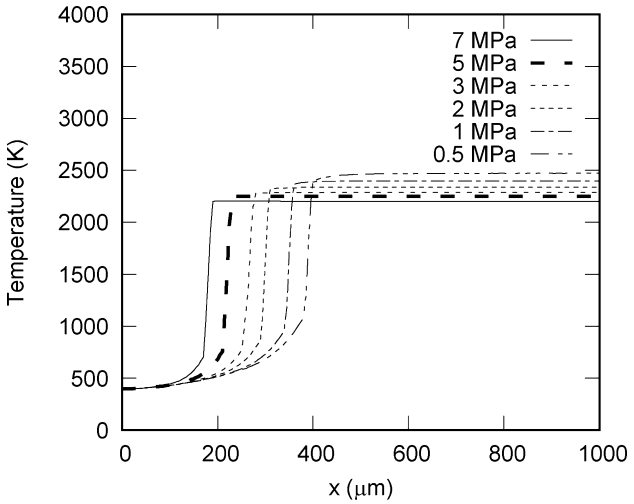

Figure 4. Temperature distribution at t = 0.04 s.

sults provided by Kohga [11] is presented in Figure 3. As shown, the results agree well for the considered pressure range. The difference between calculated and experimental results remain constant for the considered pressure range. Quantitative results and error can be seen in Table 2. The absolute error is constant with a value around 0.5 mm/s, however, the relative error increases with the decrease of the pressure due to the fall of the experimental burning rate for low pressure values.

Temperature distributions along the geometry under a pressure range from 0.5 MPa to 7 MPa are presented in Figure 4, where it can be seen how the temperature at the end of the tube increases with the fall of the pressure.

The velocity profile of the gas phase can be seen in Figure 5. The behavior of the gas velocity is opposed to the burning rate, the higher the pressure, the lower the gas velocity is. This is due to the increase of the gas density with pressure.

AP mass fraction distributions are represented in Figure 6. The content of AP multiplies as the pressure decreases. For higher pressures, AP in gas phase is located close to AP in its condensed form. However, the lower the pressure, the higher the diffusion of AP is obtained and

Table 2. Quantitative comparison of calculated and experimental burning rate.

Pressure (MPa)	OpenFoam Burning rate (mm/s)	Kohga Burning rate (mm/s)	Absolute error (mm/s)	Relative error (%)
7	7.52	7.01	0.512	7.31
5	6.61	6.08	0.537	8.84
3	5.53	5.06	0.473	9.35
2	4.82	4.39	0.437	9.96
1	3.89	3.40	0.491	14.43
0.5	3.19	2.61	0.580	22.21

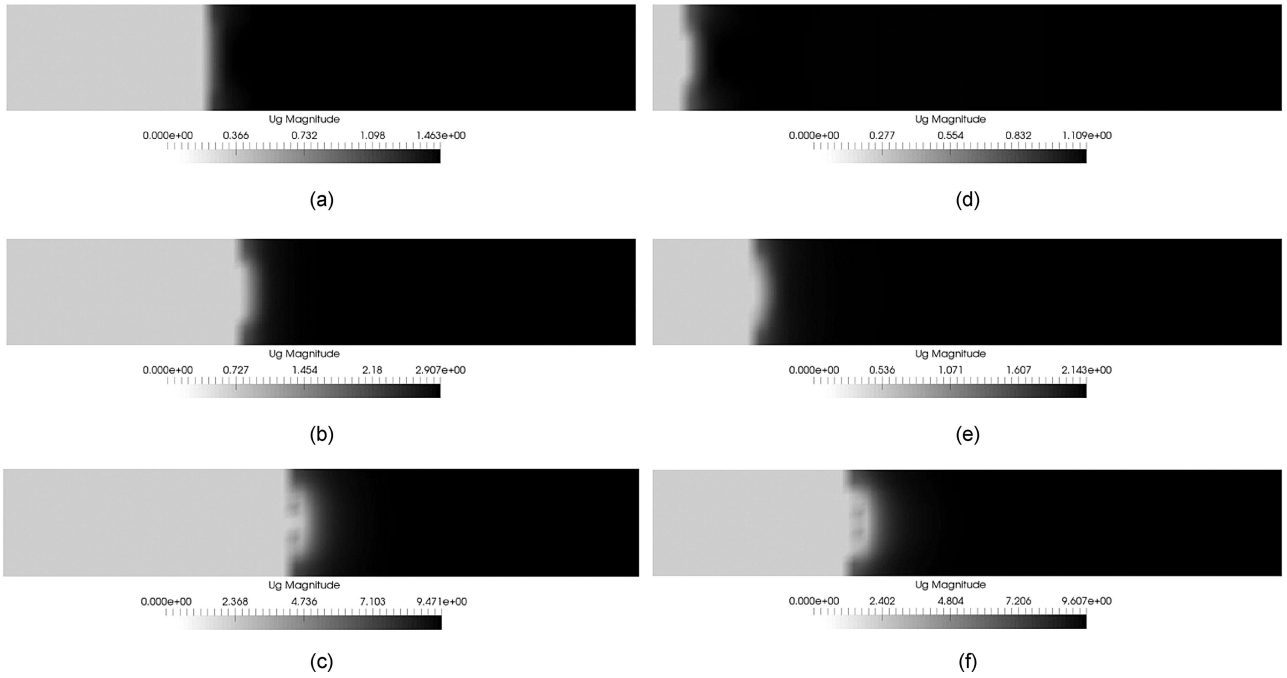

Figure 5. Velocity distribution of gas phase in t = 0.02 s at (a) 7 MPa (b) 3 MPa (c) 0.5 MPa and t = 0.06 at (d) 7 MPa (e) 3 MPa (f) 0.5 MPa.

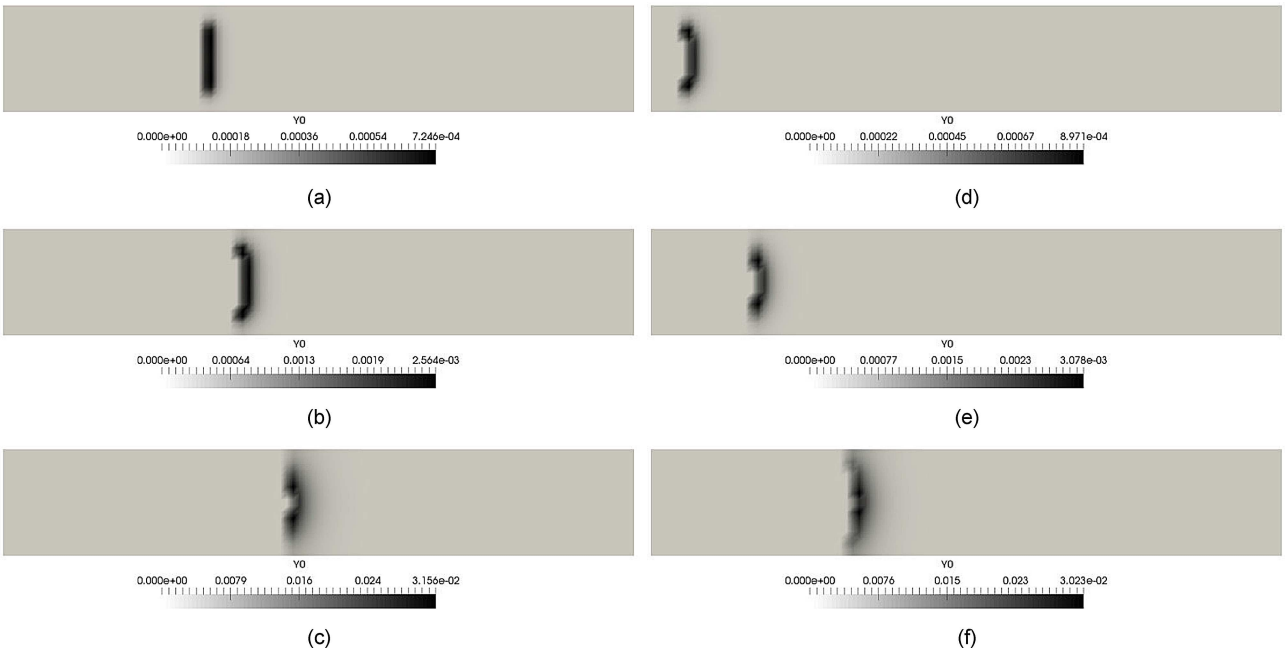

Figure 6. AP distribution in t = 0.02 s at (a) 7 MPa (b) 3 MPa (c) 0.5 MPa and t = 0.06 at (d) 7 MPa (e) 3 MPa (f) 0.5 MPa.

therefore, the number of cells which contain AP in its gaseous form increase. This behavior is due to the rise in gas velocity with the reduction of pressure which drags AP throughout the domain.

The regression rate at the burning surface and the AP and HTPB mass fractions immediately after the burning surface at 7 MPa for 0.015 and 0.065 seconds are represented in Figure 7, Figure 8 and Figure 9. As shown in Figure 9, the content of HTPB is mostly constant along y-direction. However, the content of AP (Figure 8) is minimum in the lower and upper sides of the sandwich increasing while approaching to $y = 30\ \mu m$, where it reaches its maximum and

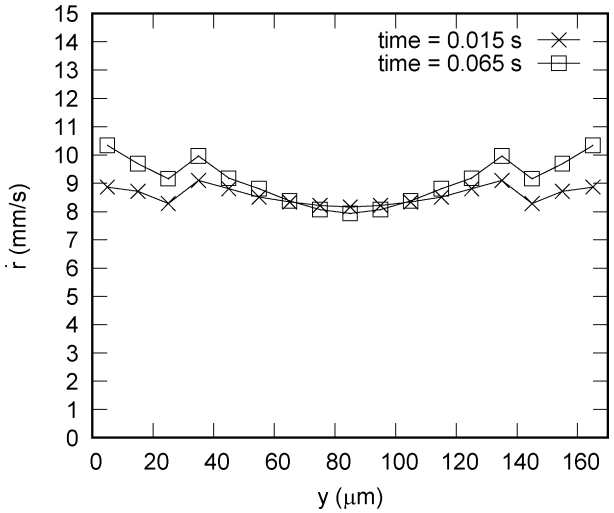

Figure 7. Burning rate distribution along the burning surface at t = 0.015 s and t = 0.065 s at 7 MPa.

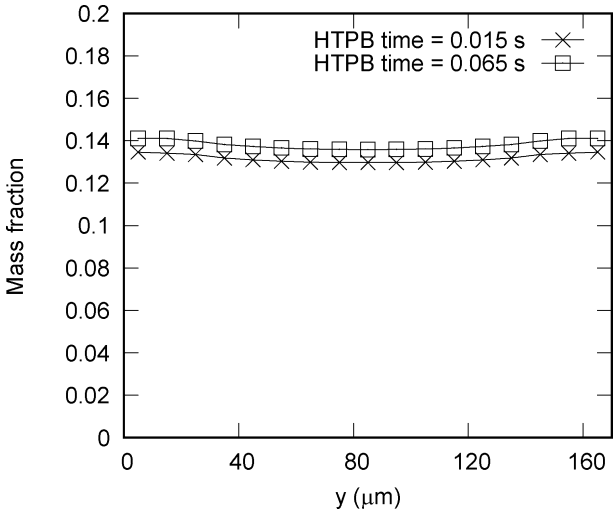

Figure 9. HTPB mass fraction distribution after burning surface at t = 0.015 s and t = 0.065 s at 7 MPa.

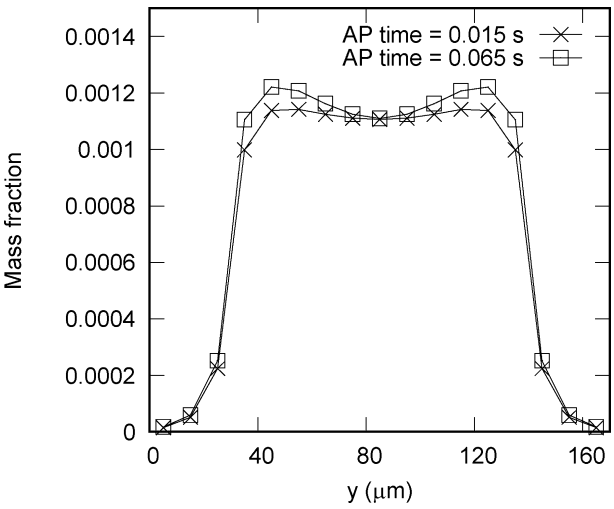

Figure 8. AP mass fraction distribution after burning surface at t = 0.015 s and t = 0.065 s at 7 MPa.

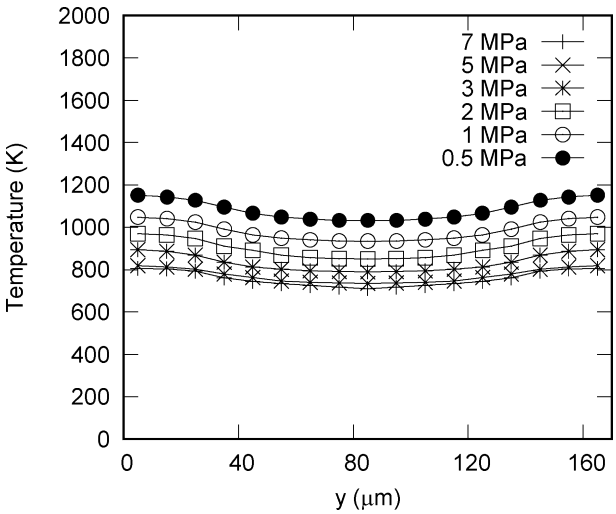

Figure 10. Temperature in condensed phase before burning surface at t = 0.03 s for 7 MPa to 0.5 MPa.

afterwards it decreases slightly until arriving to the middle of the sandwich. Figure 7 shows how the average burning rate decreases with the time. In addition, it can be observed that between $y = 30\ \mu m$ and $y = 140\ \mu m$ the profile of burning rate is similar to the one of AP mass fraction. However, in the upper and lower layers of the sandwich the burning rate is not reduced to zero, as it happens with AP content, due to the presence of HTPB in these areas which contribute to enhance the burning rate. Finally, the distribution in y-direction of condensed phase temperature at the cells adjacent to the burning surface when time is equal to 0.03 s is represented in Figure 10 for the studied pressure range. The average value of temperature decrease with the raise of pressure and its distribution is similar to the one of the regression rate at the burning surface plotted in Figure 7.

3.2 Combustion of AP/HTPB Test Tube in Crawford Bomb Strand Burner

The code was run in 2D configuration for pressures of 4 MPa and 7 MPa and initial temperatures of −53 °C, 21 °C and 74 °C. The comparison between experimental and calculated burning rate is plotted in Figure 11 and Figure 12. For both pressures, the difference between numerical and experimental results for 21 °C and 74 °C is lower than the obtained for −53 °C. In addition, it can be observed that the

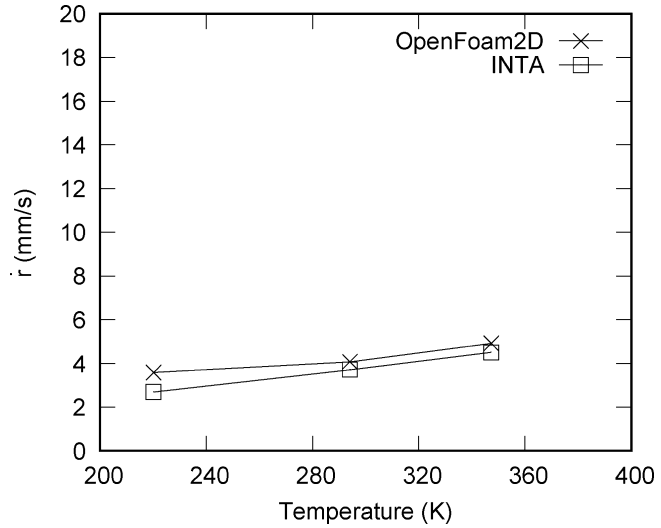

Figure 11. Comparison between calculated and experimental burning rate at 4 MPa.

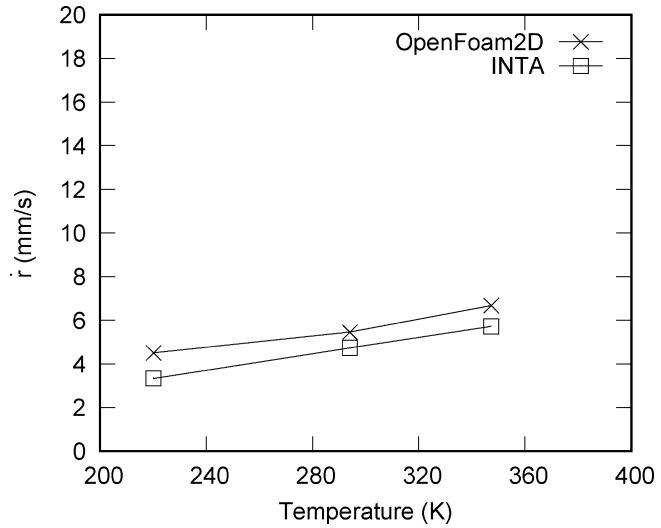

Figure 12. Comparison between calculated and experimental burning rate at HTPB mass fraction distribution after burning surface at 7 MPa.

differences between code and experimental results increase with the pressure, obtaining a better agreement for 4 MPa than for 7 MPa.

Quantitative results as well as absolute and relative errors can be found in Table 3 and Table 4. As it is shown, the absolute error is less than 1 mm/s and around 1 mm/s for 4 MPa and 7 MPa tests respectively. It is of high importance to consider the error of the experimental measurements, which can be assumed to have a value around 0.5 mm/s. The relative error increases with the decrease of temperature due to the low value of experimental burning rate at these temperatures. As a conclusion, it can be said that the results obtained with the numerical model agree with the experimental ones for the considered pressure range. The difference between calculated and experimental results remains almost constant for the considered pressure range.

Table 3. Quantitative comparison of calculated and experimental burning rate at 4 MPa.

Temperature (K)	OpenFoam Burning rate (mm/s)	INTA Burning rate (mm/s)	Absolute error (mm/s)	Relative error (%)
220.15	3.58	2.71	0.869	32.08
294.15	4.08	3.72	0.364	9.79
347.15	4.92	4.52	0.398	8.80

Table 4. Quantitative comparison of calculated and experimental burning rate at 7 MPa.

Temperature (K)	OpenFoam Burning rate (mm/s)	INTA Burning rate (mm/s)	Absolute error (mm/s)	Relative error (%)
220.15	4.52	3.34	1.180	35.34
294.15	5.45	4.75	0.704	14.83
347.15	6.68	5.73	0.949	16.57

4 Conclusions

A code to study the multi-dimensional modelling of unsteady combustion of AP/HTPB propellants has been developed in OpenFoam. Rusanov scheme and first-order Euler were used to solve the equation system and source terms.

The code was validated against two different tests. Firstly, the combustion of an AP/HTPB strand with sandwich configuration was simulated and distributions of gas velocity and AP mass fraction, as well as gas and condensed phase temperature distributions were obtained for a pressure range from 0.5 MPa to 7 MPa. The results obtained for the burning rate were compared with those from Kohga [11] obtaining the following conclusions:

1. The results obtained with the two-dimensional model implemented in OpenFoam for sandwich geometry agree with the experimental results from Kohga [11] for the considered pressure range. The absolute error is constant with a value around 0.5 mm/s. The relative error is less than 10% for a pressure range between 7 and 2 MPa and below 25% between 0.5 MPa and 2 MPa.
2. Despite of the raise of the burning rate with the pressure, the higher the pressure, the lower the gas velocity is. This behavior is due to the increase of the gas density with the pressure.
3. The content of AP in gas phase multiplies as the pressure decrease. In addition, at lower pressures, the dif-

fusion of AP is increased. This is due to the rise in gas velocity with the reduction of pressure.

4. For an established pressure, the content of HTPB in gas phase is mostly constant along y-direction. However, the content of AP is minimum in both extremes increasing while approaching to $y = 30\ \mu m$ where it reaches its maximum. Afterwards it decreases slightly until reaching the middle of the sandwich.
5. The profile of the burning rate in y-direction is similar to the one of the AP mass fraction between $y = 30\ \mu m$ and $y = 140\ \mu m$. However, in the upper and lower layers of the sandwich, the burning rate remains more or less constant due to the presence of HTPB in these areas while the mass fraction of AP decreases abruptly.

Regarding future work ideas to use the already developed mathematical model, it is considered of high importance to study the effect of the particle size together with the pressure, not only in the burning rate, but also in the temperature and AP mass fraction distributions. This analysis will be performed by varying the parameters of equations (43) and (44). By considering a fixed AP composition (α), for each chosen AP particle diameter (d_{AP}), equation (44) will provide the height of HTPB (d_{HTPB}). By introducing both values in equation (43), the total height of the control volume (L), can be obtained. Moreover, the burning rate results could be compared with the ones available in the literature, such as the ones from Jeppson and Beckstead [3] and from Kohga [11].

Afterwards, the burning of an AP/HTPB homogeneous strand in a Crawford Bomb Strand Burner at 4 MPa and 7 MPa for several initial temperatures was simulated. The comparison between the burning rate obtained by OpenFoam simulations and the experimental results provided by INTA [18] was plotted. The results obtained agree with the experimental ones for the considered pressure range. The absolute error has a value around 1 mm/s and the relative error has a value below 36% for 220.15 K and less than 10% for 294.15 K and 347.15 K at 4 MPa.

In order to improve the results obtained, it could be interesting to include the release of heat due to radiation and the emissivity of the surfaces which have been assumed neglectable when developing the mathematical model. Since the experiments are done in a closed combustion chamber, reflecting walls could be approximated as black body or gray body of high emissivity.

All in all, the benchmark results show good agreement between experimental and numerical data, not only in AP sandwich approach, but also in AP particles approach. This confirms the robustness of this kind of modelling for the prediction of AP/HTPB combustion behavior in multidimensional scenarios with transient environmental conditions such as Rocket Engines and/or base bleed units in ballistics applications.

Symbols and Abbreviations

ρ	density
$\vec{u}$	velocity
p	pressure
E	energy
k	thermal conductivity
T	temperature
c	specific heat
c_v	specific heat at constant volume
Q_g	heat of reaction
Q_c	heat of decomposition
R_g	specific constant of gases
R_u	universal constant of gases
Y	mass fraction
$\dot{r}$	burning rate
M_g	molecular mass
c_g	speed of sound
γ	heat capacity ratio
$D_{1,2}$	reaction rate constants
$n_{1,2}$	exponential pressure factor
$E_{1,2}$	activation energy
d	distance
c	condensed phase
g	gas phase
1	subscript combustion of AP
2	subscript combustion of HTPB
melt	melting
s	surface

Acknowledgements

The authors would like to acknowledge the financial support of the Spanish Ministry of Economy and Competitiveness and the European Commission (European Regional Development Fund (ERDF)/FEDER funds) throughout the ALMENA project (RTC-2016-5194-8).

References

[1] K. Kuo, M. Summerfield, Fundamentals of solid-propellant combustion in *Prog. Astronaut. Aeronaut.*, AIAA ISBN 0–915928-84-1, USA, **1984**, Vol. 90.
[2] M. W. Beckstead, R. L. Derr, C. F. Price, A model of composite solid-propellant combustion based on multiple flames, *AIAA J.* **1970**, *8,* 2200–2207.
[3] M. B. Jeppson, M. W. Beckstead, Q. Jing, A kinetic model for the premixed combustion of a fine AP/HTPB composite propellant, *36th AIAA Aerospace Sciences Meeting and Exhibit, Aerospace Sciences Meetings* **1998**.
[4] C. Guirao, F. A. Williams, A model for ammonium perchlorate deflagration between 20 and 100 atm, *AIAA J.* **1971**, *9*, 1345–1356.
[5] G. M. Knott, M. Q. Brewster, Modelling the combustion of propellant sandwiches, *Comb. Sci. Technol.* **2002**, *174.* 61–90.
[6] Y. J. Cao, Y. G. Yu, R. Ye, Numerical analysis of AP/HTPB composite propellant combustion under rapid depressurization, *Appl. Therm. Eng.* **2015**, *75*, 145–153.

[7] W. Cai, V. Yang, A model of AP/HTPB composite propellant combustion, *AIAA* **2000**, 2000–0311.
[8] W. Cai, P. Thakre, V. Yang, A model of AP/HTPB composite propellant combustion in rocket-motor environments, *Comb. Sci. & Tech* **2008**, *180*, 2143–2169.
[9] J. A. Moríñigo, J. Hermida-Quesada, Evaluation of reduced-order kinetic models for HTPB-oxygen combustion using LES, *Aerospace Science and Technology* **2016**, *58*, 358–368.
[10] Y. G. Yu, Y. H. Zhou, C. Y. Lu, X. C. Xue, Study on Unsteady Combustion Behaviors of AP/HTPB Base-Bleed Propellants under Transient Depressurization Conditions, Propellants, Explosives, *Pyrotechnics* **2014**, *39*, 511–517.
[11] M. Kohga, Burning Characteristics and Thermochemical Behavior of AP/ HTPB Composite Propellant Using Coarse and Fine AP Particles, *Propellants Explos. Pyrotech.* **2011**, *36*, 57–64.
[12] N. Kubota, *Propellants and Explosives: Thermochemical Aspects of Combustion* in WILEY-VCH Verlag GmbH& Co. KGaA, Germany, **2001**.
[13] F. Miccio, Numerical modeling of composite propellant combustion , *Symposium (International) on Combustion* **1998**, *27*, 2387–2395.
[14] F. Favale, F. Miccio, Modeling unsteady and perturbed combustion of heterogeneous composite Propellants, *Aerospace Science and Technology* **2008**, *12*, 285–294.
[15] E. F. Toro, *Riemann Solvers and Numerical Methods for Fluid Dynamics*, Springer, **1997**.
[16] V. Rusanov, Calculation of Interaction of Non-Steady Shock Waves with Obstacles, *USSR Computational Mathematics and Mathematical Physics* **1961**, *1*, 267–279
[17] J. R. García-Cascales, R. A. Otón-Martínez, F. J. S. Velasco, F. Vera-García, A. Bentaib, N. Meynet, Advances in the characterisation of reactive gas and solid mixtures under low pressure conditions, *Comput. Fluids* **2014**, *101*, 64–87.
[18] Ensayos de la velocidad de combustión. Instituto Nacional de Ténica Aeroespacial (INTA). Ministerio de Defensa.
[19] X. Zhou, T. L. Jackson, J. Buckmaster, A numerical study of periodic sandwich propellants with oxygenated binders, *Combust. Theory Modell.* **2003**, *7*, 435–448.
[20] R. Ye, Y. G. Yu, Y. J. Cao, Analysis of Micro-scale Flame Structure of AP/HTPB Base Bleed Propellant Combustion, *Defence Technology* **2013**, *9*, 217–223.

Manuscript received: February 1, 2019
Revised manuscript received: April 25, 2019
Version of record online: August 26, 2019

